

INVESTIGATIONS OF THE PRESSURE SHOCK-WAVE GENERATED BY H.B.C. STRIP FUSE ELEMENTS AT THE ARC-IGNITION INSTANT IN SAND FILLED FUSES

J.Hibner, T.Lipski
Gdańsk Technical University, Gdańsk
Własna Strzecha 18 a
Poland

Abstract

The paper describes laboratory investigations of the pressure exploding component generated at the instant of the arc-ignition instant in h.b.c. fuse-elements. 3 different strip shapes of the fuse-elements were applied. Also 4 thicknesses and 5 widths of those strips were used. Tests in a l.v. short-circuit test's rig were carried out using 2 different h.b.c. model fuses. As an arc-quenching medium the standard sand of l.v. fuses was utilized. The test results show some distinct influence of the constiction number, strip length and its width. Test results are illustrated by the oscillograms and the profiles of above mentioned relations. The conclusions end the paper.

1. Introduction

The pressure generation during electrical conductor explosion is known from many years. For example the recorded pressure of order 100 MPa was not so seldom case, if a wire was exploded in the water [5]. Electrical explosion investigators usually are speaking about so-called exploding component [2] of the pressure, because the whole energy delivered to the exploding conductor responsible is for that pressure. On the contrary in h.b.c. fuses, in which a fuse-element is placed in quartz sand during arcing, two pressure components are generated [6]: one, exploding component, at the instant of the arc-initiation due to fuse-element initial explosion (usually in constrictions); second one, arcing component, as a result of delivering of the energy to the arc-column. The superposition of those both components is responsible for an exposure of the fuse-link body onto eventual damage due to mechanical failure.

Because both mentioned components are acting in completely different time spans the peak of the superimposed pressures equals to the peak of the one or another component. The time duration of the explosive component is of order hundreds microseconds whereas of the arcing one equals to the arcing-time, say several milliseconds. The explosive component usually is oscillatory one with a strong pronounced damping mainly by sand, while the arcing pressure follows approx. after cumulative effect of the liberated arc-energy. The explosive component, upon suggestion given in [6], depends on some power of the current density in the explosion instant. And, of course, due to good damping ability of the sand the pressure magnitude on the fuse-link body is much smaller than that in the exploding constriction.

Published results [3] on the explosive component are dealing with the uniform Cu wire fuse-element of diameter 0.5 mm and length 20 mm stretched in the sand. From the manufacturing point of view, however, more interesting should be the pressure behaviour in h.b.c. fuses equipped within strip elements having some constricted parts. This need became the base why since 1977 in our Institute a number of the measurements were done on the pressure in some model h.b.c. fuses with the strip elements. Some results of those investigations limited just to the exploding component are reported hereinafter. Everywhere in the following text speaking about the pressure one shall understand the exploding component of the pressure.

2. Experiments

2.1 Test circuit

To get the most reproducible conditions of the tests using AC current a thyristor making-switch has been used of 1 kA continuous rated current and 2 kV peak reverse rated voltage, shown in Fig.1. A coaxial practically noninductive shunt of 1 or 5 m Ω rated resistance serves to the current measurements. A cathode 5 beam oscillograph of 0.5 M Ω and 40 pF input constants enabled the records of the interested parameters. During check-out procedure of the measuring system a 2 beam oscillograph of 1 M Ω and 40 pF input parameters found an app-

lication.

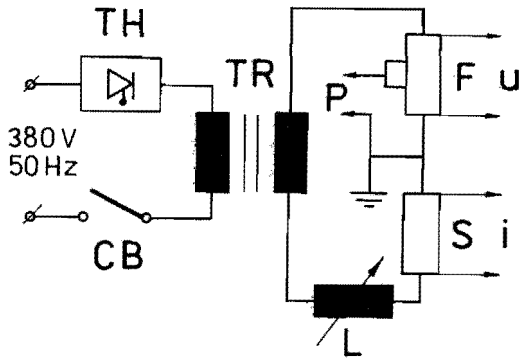


Fig. 1 Simplified test's circuit
 TH - making switch, CB - safety circuit-breaker, TR - transformer 380/260 V or 520 V, L - choke, F - tested fuse, S - shunt, u, i, p - recorded voltage, current, pressure

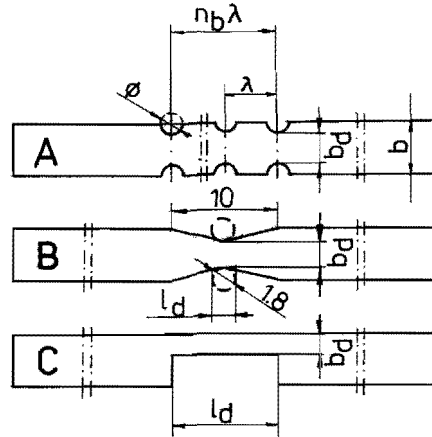


Fig. 2 Tested fuse-elements

2.2 Fuse-elements

The strip fuse-elements of the different shapes shown in Fig.2, of the thicknesses 0.05, 0.1, 0.185 mm and of the widths 3.1, 5, 7.5, 10, 15 mm were applied. The constrictions were distributed rhythmically along the fuse-element with-

in modulus λ . Fuse-element type C has got a rectangular cutting out of the different length.

2.3 Model fuse-links

Two different kinds of the h.b.c. model fuse-links were used, body of which were made from some organic textolite. The body of one was tight, made from one piece (Fig.3a). The fuse-element in this case was soft soldered to the terminals. Arc-quenching chamber, - 16 mm. The second one (Fig.3b) has got the chamber diameter 26 mm within lengthwise divided body, fastened by 4 screws M5. The fuse-element now is clamped to the terminals by the wedge fasteners. In every case as an arc-quenching medium the quartz sand of 0.3+0.5 mm granularity has been used. The granularity fractions were : ab. 67 % of 0.385+0.43 mm and ab. 22 % of 0.43+0.49 mm. The fuse-elements were situated along the cylindrical arc-chamber axis. A standard firm procedure of the sand gave in result ab 16 % of the mass increment in relation to the loose sand in the chamber.

2.4 Pressure sensor

A piezoelectric sensor has been used of the sensitivity 1.88 V/MPa, self-capacity 900 pF and resistivity 600 GΩ. The measured frequency range up to 100 kHz. A concentric cable of ϕ 7 mm and of 5 m length to connect the sensor with oscillograph was applied. The wave resistance of the cable, - 75Ω. The check-out tests of the presure

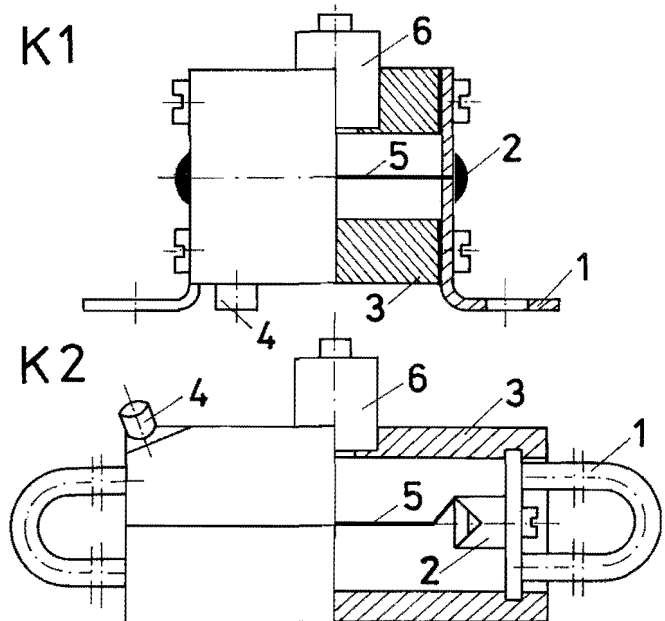


Fig. 3 Tested fuse-links
 K1 - chamber ϕ 16 mm, length 42 mm; K2 - chamber ϕ 26, length 64 mm; 1 - terminal; 2 - fuse-element connection; 3 - body; 4 - hole for sand strew in closed by nut M8X1 mm; 5 - fuse-element; 6 - p-sensor of ϕ 8 mm surface

measuring system has showed no practical influence of the interferences.

3. Test results

Pressure test results show relatively great dispersion, that's why to determine an average magnitude it was necessary to make atleast 10 measurements. Some exemplary results indicated in the Fig.4 show that the exploding pressure component lasts less than 100 μ s.

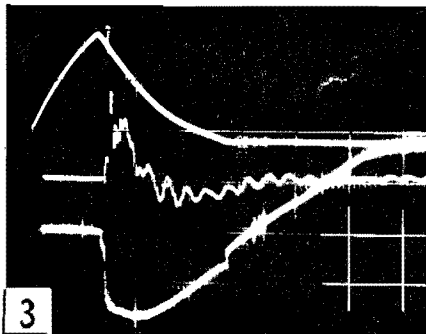
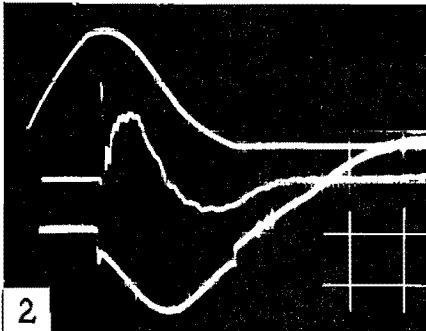
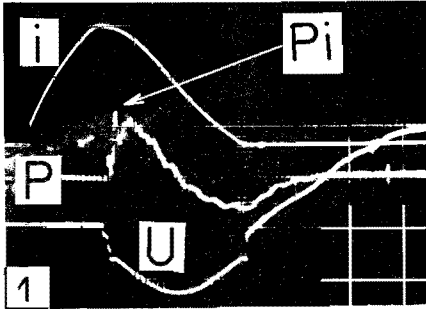


Fig. 4 Exemplary test records of fuse-links K2, circuit conditions 520 V, 50 Hz. 1 -element A, $n_b = 3$, constrictions $\phi = 1.8$ mm, $\lambda = 3$ mm; 2 - element C, $l_d = 5$ mm; 3 - as 2 but $l_d = 20$ mm. Scale unit 746 A/cm, 216 V/cm, 0.216 MPa/cm, 1.5 ms/cm

Obtained results are summarized in the Figs 5 to 9. Given in those Figures exemplary profiles are for this same constriction cross-sectional area. Due to the adiabatic heating conditions kept during the tests in every case the current density at the instant of the arc-initiation was practically this same. From Figures 5 to 8 outcomes that the influence of the parameters n_b , b_d , and l_d on the pressure is weakening with their growing according to the rule

$$p_i = \frac{P_{max}}{1 + \frac{k}{x}} \quad (1)$$

in which x is one of the variable n_b , b_d , l_d . For example in the case of pressure relation on the length l_d from the experiments follows

$$p_i = \frac{0.8}{1 + \frac{10}{l_d}} \quad (2)$$

where p_i in MPa, l_d in mm. From (2) it is clear that further the exploding part to the measuring point lesser its influence on the pressure measured. It can be showed that the relation (1) is in agreement with some analytical calculations based on sum of the partial pressures along the fuse element. The profile given in Fig.7 indicates, for instance, that already for $l_d > 25$ mm the pressure in the centre of the fuse-link has got nearly maximum value, but not so much higher than for 10 mm.

Data in Fig.9 suggest that there is not any logical relation. That's why the arc-ignition voltage can not be the base for the pressure calculation, despite that voltage relates to the length l_d and current density as follows

$$u_i = \rho l_d \sqrt{j} \quad (3)$$

In addition to that it is necessary to admit that given in the Figure 9 magnitudes are practically for this same current density in the instant of explosion. The results show also (Table 1) that despite 1.8 greater current in the instant of explosion the pressure changes are small. This changes are of order of the result dispersion. But to underline is nearly this same current density at that instant. To note is as well that for every couple of results the circumference of the constriction was practically this same. The only change in both results of given couple was the difference of the thicknesses, i.e. 0.1 or 0.2 mm.

Aforementioned results suggest the pressure exploding component can be described as follows

$$P_i = k_p (b_d l_d)^{\beta} j_i^{\alpha} \quad 2(\alpha - \beta) \quad (4)$$

where p_i - in MPa; k_p - in $\frac{MPa \cdot mm}{A^{\alpha}}$ depends on the chamber diameter, sand porosity and granularity; b_d , l_d - in mm; j - current density in A/mm^2 ; α, β - some powers.

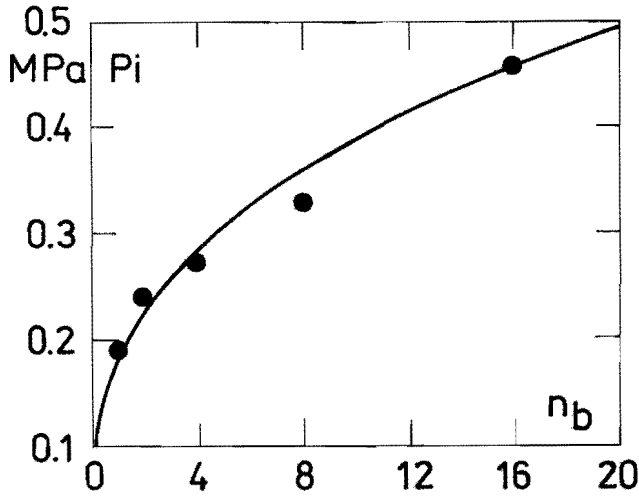


Fig. 5 p_i versus n_b for element A, fuse-link K1, 260 V, 50 Hz

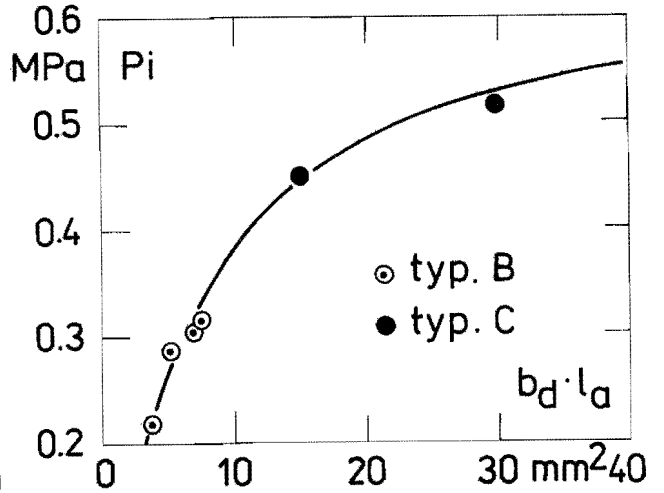


Fig. 8 p_i versus product $b_d \cdot l_d$ for element B and fuse-link K2 and element C and K2, 260 V, 50 Hz

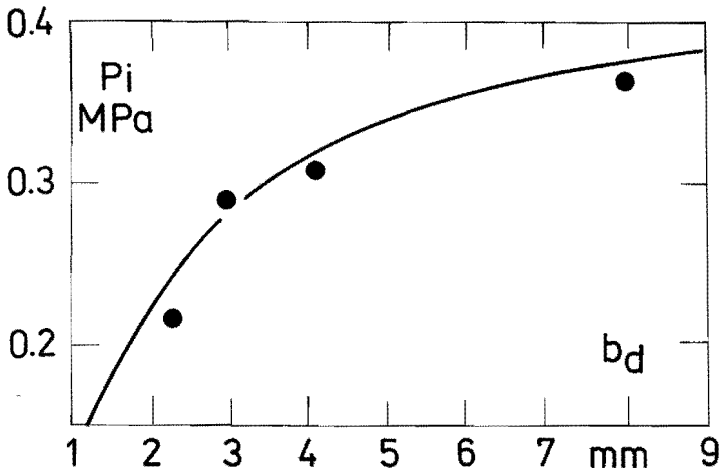


Fig. 6 p_i versus b_d for element B, fuse-link K2, 260 V, 50 Hz

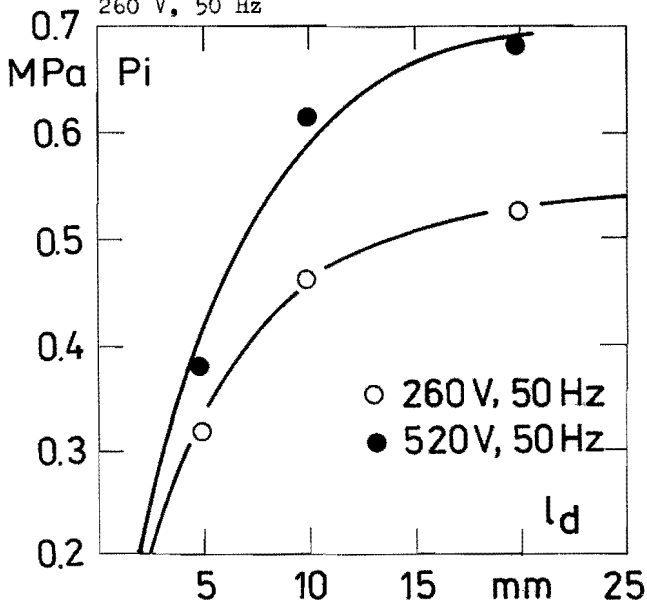


Fig. 7 p_i versus l_d for element C, fuse-link K2, 260 V and 520 V, 50 Hz

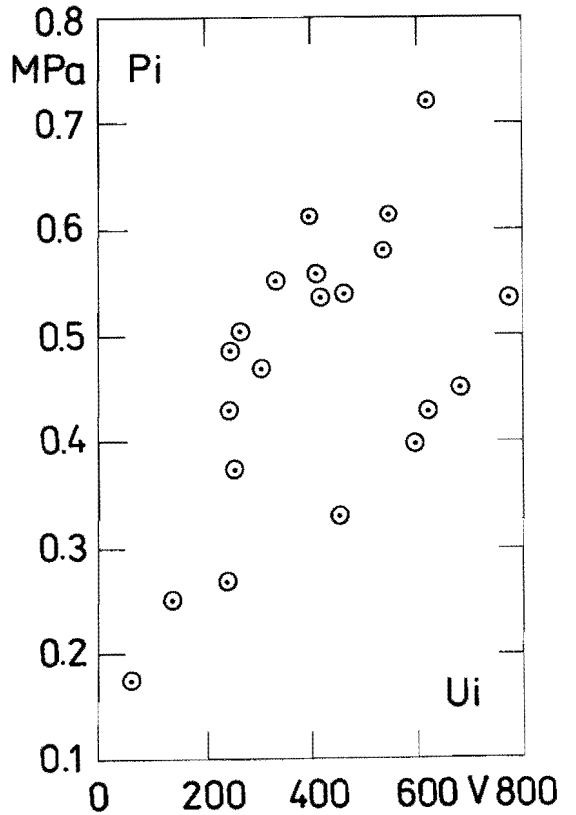


Fig. 9 p_i versus arc-ignition voltage u_i for elements A, B, C, fuse-link K2, 260 V, 50 Hz

The relation (4) relates to the tested fuse-link models, applied filler and moreover in the case of fuse-element C to the length $l_d = 10$ mm and it is valid for single element placed in the fuse-link axis in such a way that the flat surface is parallel to the measuring surface of the pressure sensor.

As the preliminary result it is stated that the powers α, β for those conditions are in the limits $0.5 + 1.0$.

Table 1 Influence of i, j, u_i on p_i

| λ mm | n_b - | ϕ mm | S_{d2} mm ² | i A | j A/mm ² | u_i V | p_i MPa | p_i % | i % |
|-----------------|------------|--------------|-----------------------------|----------|--------------------------|------------|--------------|------------|----------|
| 3 | 3 | 1.8 | 0.15 | 1603 | 10686 | 253 | 0.328 | 100 | 100 |
| 3 | 3 | 1.8 | 0.30 | 2727 | 9090 | 250 | 0.392 | 120 | 170 |
| 6 | 3 | 4.3 | 0.15 | 1515 | 10100 | 305 | 0.370 | 100 | 100 |
| 6 | 3 | 4.3 | 0.30 | 2727 | 9090 | 341 | 0.455 | 123 | 180 |
| 6 | 5 | 4.3 | 0.15 | 1515 | 10100 | 538 | 0.477 | 100 | 100 |
| 6 | 5 | 4.3 | 0.30 | 2727 | 9090 | 449 | 0.506 | 106 | 180 |

Note: given in the Table magnitudes are for elements A, fuse-link K1.

4. Conclusions

- A. The exploding pressure component lasts very short time (range of μs) and appears during explosion.
- B. It can be assumed that in given design the exploding component depends on the fuse-element dimensions of its that part which explodes. As a parameter is the current density at the instant of arc-ignition and the circumference of the fuse-element in the place of explosion.

- C. When a fuse-element does disintegrate along the whole its length the pressure exploding component is a maximum in the middle of the fuse-link. From the relation (2) it can be seen that the influence of some further parts is lesser on the generated pressure.
- D. It seems, the exploding pressure component in described measurements depends on the current density rather than current magnitude in the instant of arc-initiation. For example by ab 1.8 times greater current the pressure remains nearly this same by nearly this same current density.
- E. It seems, the exploding pressure component does not depends on the arc-ignition voltage. The problem needs some further investigations.
- F. The practical calculation of the exploding pressure component, it seems, could be possible from the relation (4). But to get more precise results it is necessary to carry out further investigations to establish appropriate magnitudes of the powers α and β .

5. Acknowledgement

The authors wish to thank Mrs.D.Piotrzkowska, Mr.P.Piotrzkowski and Mr.A.Bartus for their valuable contributions to the pressure measurements.

6. References

- [1] Baxter H.W. 1950, Electric Fuses, Edward Arnold and Co Ed. London.
- [2] Exploding Wires. Vol. 1-4, W.G.Chace and H.K.Moore Eds. New York, Plenum 1964.
- [3] Gul A., Lipski T. Pressure shock-wave investigations during the wire-element explosion in a h.b.c. fuse. Switching Arc Phenomena Int.Symp. Łódź, Poland, 1985. P.I: Conf Materials p.326-330.
- [4] Hibner J. Calculation of the arc-ignition voltage of the fuse-elements with rectangular constriction (in Polish). Przegląd Elektrotechniczny. 1978, No.5, p.204-206.
- [5] Krsavage J. In Exploding Wires. Vol. 2, W.G.Chace and Moore Eds. New York, Plenum 1964.
- [6] Lipski T. Generation and propagation of the pressure due to the fuse-element disintegration in h.b.c. fuses. Gas Discharges and Their Applications, Int. Conf. Oxford, 1985, p.87-90.

A ONE DIMENSIONAL MATHEMATICAL MODEL FOR THE DYNAMICAL BURNBACK VELOCITY OF SILVER STRIPS

J.G.J. Sloot and V.K.I Kalasek
 Department of Electrical Engineering
 Eindhoven University of Technology.

J. Sikkenga
 Holec Systems & Components
 Hengelo

Abstract

This article presents a one dimensional numerical model for the burn-back process, including changes of a metal strip under the influence of an arc. Special attention is given to the velocity decrease caused by heat conduction and the velocity caused by Joule preheating.

Introduction.

In a short circuit situation, the arc voltage increase of a fuse is dominated by the burn-back velocity of the metal strip. Early investigations of Kroemer [1] showed a linear dependence between the velocity v and the current density j of the strip:

$$v = kj \dots \dots \dots (1)$$

with $k = 1.15 \text{ E-}9 \text{ [m}^3/\text{As]}$

Daalder [2] suggested an expression for the burning constant k :

$$k = \frac{U}{H_{\text{drop}} - H_{\text{begin}}} \dots \dots \dots (2)$$

with

$$H_{\text{begin}} = c_s \gamma T_{\text{begin}} \dots \dots \dots (3)$$

$$H_{\text{drop}} = c_s \gamma T_{\text{melt}} + \gamma L + c_l \gamma (T_{\text{drop}} - T_{\text{melt}}) \dots (4)$$

In these formulas:

- U: power loss per A arc current to the electrode.
- H_{drop} : the maximal specific enthalpy of a metal part, before it is removed by the arc.
- H_{begin} : the already reached local enthalpy when the arc arrives.
- C_s, C_l : specific heat of the metal in the solid and liquid state.
- γ : specific density in the solid state.
- L: melting heat.
- T_{melt} : melting temperature.
- T_{drop} : temperature of liquid droplets.
- T_{begin} : initial temperature of the metal spot when the arc arrives.
- T_o : room temperature.

Because of Joule heating, T_{begin} can be considerably higher than T_o . For an adiabatic situation, T_{begin} was calculated from:

$$T_{\text{begin}} = T_o \exp\left(\frac{j^2 t L_{\text{wf}}}{\lambda \gamma c_s}\right) \dots \dots \dots (5)$$

where $L_{\text{wf}} = \frac{\lambda \rho}{T}$ stands for the constant of Wiedemann-Franz, with λ for the thermal conductivity and ρ for the electrical resistivity.

Equation (2) fits a part of the experimental results of Daalder [2] with silver, under the assumption that $U = 5.25 \text{ V}$ and $T_{\text{drop}} = 1700 \text{ K}$. However experimental velocities at current densities above 3 kA/mm^2 and arcing times of about 5 ms , could not be described with equation (2) as T_{begin} would exceed T_{melt} . Therefore, our first aim was to extend the validity of equation (2) up to higher current densities.

The most simple extension can be reached by allowing H_{begin} to exceed the product $C_s \gamma T_{\text{melt}}$. In this case the enthalpy increase by Joule heating can be calculated with:

$$\frac{dH}{dt} = \rho j^2 \dots \dots \dots (6)$$

where for the solid or liquid phase:

$$\frac{dH}{dt} = \gamma c \frac{dT}{dt} \dots \dots \dots (7)$$

or for the melting phase:

$$\frac{dH}{dt} = \gamma L \frac{df}{dt} \dots \dots \dots (8)$$

with fraction $f < 1$

4. Discretisation and assumptions.

The elements are numbered $N = 1 \dots N_{tot}$, with $L_{band} = N_{tot} dx$.

- N=1: between $x=0$ dx and 1 dx
- 2: .. 1 dx and 2 dx
- N: .. (N-1)dx and N dx
- L: .. (L-1)dx and L dx, the first liquid element
- M: .. (M-1)dx and M dx, the first melting element
- S: .. (S-1)dx and S dx, the first solid element

The time is also discretized: time $t = Kdt$, with step number $K=0 \dots K_{tot}$.

A number of assumptions will be made to transform the set of integral equations into linear equations:

- a) As the temperature in the whole element, the mean temperature within an element between x and $x+dx$ is defined:

$$\int_{x=(N-1)dx}^{x+dx} T(x,t) dt = T \frac{K}{N} dx \dots \dots \dots (12)$$

- b) For the heat conduction it is assumed:

$$\int_t^{t+dt} \lambda \left[\frac{dT}{dx} \right]_x dt = \lambda \left(T \frac{K}{N} - T \frac{K}{N-1} \right) \frac{dt}{dx} \dots \dots \dots (13)$$

The temperature dependence of λ is taken into account using different values for the solid, liquid and melting phase with indexes 1,2,3 respectively.

For the integral equation the relevant value at element N-1 is chosen.

- c. During the melting the mean enthalpy in an element is taken:

$$\int_x^{x+dx} \gamma H(x,t) dx = \gamma H \frac{K}{N} dx \dots \dots \dots (14)$$

- d. The temperature dependence of the specific electrical resistivity is taken into account by the resistivity factor A:

$$A = \frac{\rho}{\gamma c T} \dots \dots \dots (15)$$

with $A=A1$ for the solid phase.
 $A=A2$ for the liquid phase.
 $\rho = \rho_{melt}$ for the melting phase.

The Joule heat development in an element during dt can be expressed as:

$$\int_t^{t+dt} \int_x^{x+dx} \rho j^2 dx dt = A \gamma c j^2 dx dt T \frac{K}{N} \dots \dots \dots (16)$$

- e. It is assumed that the liquid arc front element is removed on a certain moment t_1 if:

$$\int_{x_1}^{x_1+dx} c \gamma T(x, t_1) dx > c \gamma T_{drop} dx \dots \dots \dots (17)$$

If the last but one arc front element has been removed at time t_2 , the instantaneous burnback velocity during the time range t_1-t_2 is defined as :

$$v_{mom}(t_1, t_2) = dx / (t_1 - t_2).$$

- f. The melting front element has been melted at time t_1 , if:

$$\int_{x_m}^{x_m+dx} \gamma H(x, t) dx > \gamma H_{melt} dx \dots \dots \dots (18)$$

The melting border then moves from x_m to $x_m' = x_m + dx$.

- g. The initial temperature of the silver strip is T_0 .

The temperature of the fixed end remains constant $T = T_0$.

5. Sets of linear equations.

The integral equations now can be transformed into a set of linear equations. A number of substitutions will be introduced to reduce the length of the equations:

$$P_1 = \frac{P dt}{c \gamma dx}$$

$$B_1 = j^2 A_1 dt \quad B_2 = j^2 A_2 dt \quad B_3 = \frac{j^2 \rho_{melt} dt}{\gamma}$$

$$G_1 = \frac{\lambda_1 dt}{\gamma c dx^2} \quad G_2 = \frac{\lambda_2 dt}{\gamma c dx^2} \quad G_3 = \frac{\lambda_3 dt}{\gamma c dx^2}$$

- a. The liquid range with $L < N < M$.

The energy balance of the liquid front element L now can be described by:

$$T_L^{K+1} = (1 + B_2 - G_2) T_L^K + G_2 T_{L+1}^K + P_1 \dots \dots \dots (19)$$

and the other liquid elements with $L+1 \leq N < M$:

$$T_N^{K+1} = G_2 T_{N-1}^K + (1 + B_2 - 2G_2) T_N^K + G_2 T_{N+1}^K \dots \dots \dots (20)$$

- b. The melting range, with $M < N < S$.

The element M on the melting front, when it is bounded by the arc:

$$H_M^{K+1} = H_M^K + B_3 + c P_1 - c G_3 (T_M^K - T_{M+1}^K) \dots \dots \dots (21)$$

If the melting front element M is bounded by liquid material:

$$H_M^{K+1} = H_M^K + B_3 + cG_2(T_{M-1}^K - T_M^K) - cG_3(T_M^K - T_{M+1}^K) \dots (22)$$

The other elements of the melting range.

$M+1 \leq N < S$:

$$H_N^{K+1} = H_N^K + B_3 - cG_3(T_{N-1}^K - 2T_N^K + T_{N+1}^K) \dots (23)$$

c. The solid range with $S < N < N_{tot}$

If the solid front element S is bounded by the arc:

$$T_S^{K+1} = (1 + B_1 - G_1)T_S^K + G_1T_{S+1}^K + P_1 \dots (24)$$

If the solid front element S is bounded by melting material:

$$T_S^{K+1} = G_3T_{S-1}^K + (1 + B_1 - G_3 - G_1)T_S^K + G_1T_{S+1}^K \dots (25)$$

If the solid front element S is bounded by liquid material:

$$T_S^{K+1} = G_2T_{S-1}^K + (1 + B_1 - G_2 - G_1)T_S^K + G_1T_{S+1}^K \dots (26)$$

The other elements in the solid state:

$S+1 \leq N \leq N_{tot}$

$$T_N^{K+1} = G_1T_{N-1}^K + (1 + B_1 - 2G_1)T_N^K + G_1T_{N+1}^K \dots (27)$$

| | | |
|---------------------------------------|-------------------------|----------------------|
| metal | : silver | |
| melting temperature | : $T_{melt} = 1234$ | [K] |
| mass density | : $\gamma = 1.05E4$ | [kg/m ³] |
| specific heat | : $C = 270$ | [J/kg] |
| specific resistivity at T_{melt} | : $\rho_{melt} = 13E-8$ | [Ω] |
| resistivity factor below T_{melt} | : $A_1 = 2.1E-17$ | [Ω^2/J] |
| resistivity factor above T_{melt} | : $A_2 = 4.4E-17$ | [Ω^2/J] |
| melting heat | : $L_{melt} = 1.045E5$ | [J/kg] |
| thermal conductivity below T_{melt} | : $\lambda_1 = 395$ | [W/mK] |
| above T_{melt} | : $\lambda_2 = 185$ | [W/mK] |
| at T_{melt} | : $\lambda_3 = 290$ | [W/mK] |
| length of the half of silver strip: | $L_{band} = 40E-3$ | [m] |
| power loss per ampere to electrode: | $U_{con} = 5.25$ | [V] |
| temperature of liquid droplets | : $T_{drop} = 1700$ | [K] |

Table 1. Variables of the numerical model.

6. Results of the calculations.

The set of linear equations with the distinct conditions were assimilated in a relatively simple computer program, with PASCAL and FORTRAN versions, suitable for personal computers.

Time steps were chosen in accordance with the usual stability limits for the explicit solution method of the diffusion equation. Material properties were chosen in accordance with table 1.

The values for U_{con} and T_{drop} were chosen in according [2], although other combinations are quite possible.

The output results of the program can be characterized by normalized time-distance diagrams like Fig. 2. It shows the physical state history of any silver part; the length coordinate and the time are divided by the strip length and the total current period respectively.

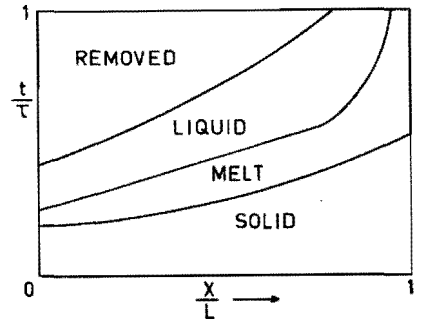


Fig. 2 Normalized diagram of the dynamic burnback process.

To illustrate the influence of the Joule heating and the heat loss by conduction the instantaneous burnback velocity was calculated for several constant current densities during a period of 5-10 ms. Some results are presented in Fig. 3.

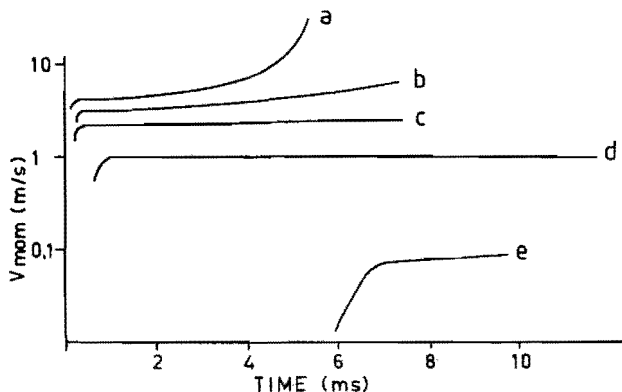


Fig. 3. Calculated dynamical burnback velocities.

| current density [kA/mm ²] | pre arcing time [ms] |
|--|-------------------------|
| a: 4.04 | 0.1 |
| b: 3.18 | 0.2 |
| c: 2.10 | 0.1 |
| d: 1.02 | 0.6 |
| e: 0.10 | 0.0 |

It is assumed that the arc is initiated after a 'pre-arcing time', during which the Joule heat source is already active. Fig. 3 shows that for the lowest current density ($j=0.1$ kA/m²), the heat loss by conduction can even prevent the burnback for several ms. In this case non-infinitely thin melting layers occurred at the start of the process.

In the intermediate current density range 1-2 kA/mm², the instantaneous velocity reaches the stationary value within a fraction of a ms.

At higher current densities the Joule heating can cause an exponential increase of the burnback velocity, but this forms no principal limit for the model validity.

Different from the low current situation, melting layers now appeared at the end of the movement process.

Fig. 2 presents instantaneous values, integration is needed when mean velocities have to be considered, which can be compared with experimental results.

In table 2 some experimental and calculated results of Daalder [2] are compared with our numerical program results for the mean velocity.

| current density [kA/mm ²] | pre-arcing time [ms] | arcing time [ms] | mean velocity | | |
|--|-------------------------|---------------------|------------------|-------------------|-------------------|
| | | | exp [2] [m/s] | calc [2] [m/s] | pro-gram [m/s] |
| 0.10 | 0.0 | 10.0 | --- | 0.1 | 0.04 |
| 1.02 | 0.6 | 11.8 | 1.3 | 1.1 | 1.1 |
| 1.40 | 0.0 | 11.6 | 1.4 | 1.5 | 1.5 |
| 1.61 | 0.6 | 11.8 | 1.8 | 1.8 | 1.8 |
| 2.10 | 0.1 | 7.4 | 2.4 | 2.4 | 2.3 |
| 2.30 | 0.6 | 10.9 | 2.7 | 3.0 | 2.9 |
| 2.59 | 0.3 | 9.3 | 3.1 | 3.4 | 3.3 |
| 2.78 | 0.3 | 5.5 | 3.0 | 3.3 | 3.2 |
| 2.96 | 0.3 | 6.0 | 3.7 | 3.7 | 3.6 |
| 3.18 | 0.2 | 7.2 | 4.0 | * | 4.5 |
| 3.26 | 0.3 | 5.8 | 4.0 | 4.4 | 4.2 |
| 3.28 | 0.2 | 7.1 | 3.7 | * | 5.1 |
| 3.64 | 0.2 | 5.6 | 4.7 | * | 5.4 |
| 3.96 | 0.1 | 5.4 | 4.2 | * | 7.4 |
| 4.04 | 0.1 | 5.2 | 4.9 | * | 7.7 |

Table 2. Comparison between experiment, mean burnback velocities according [2] and the numerical program results, with N=500 and time step $\Delta t = 1E-6$ sec.

For $j=0.1$ kA/mm² Table 2 shows that a considerably lower value for the mean velocity is expected with the program, when compared with the result of the stationary equation according [2]. This difference obviously is caused by the retarding influence of the heat loss by conduction. Unfortunately no experimental data were available to test the 0.1 kA/mm result.

An agreement can be noticed for the higher current density range until 3 kA/mm .

For the highest current densities the former calculation [2] is not valid, as T_{begin} exceeds T_{melt} ; this is indicated in table 2 by an asterisk (*). The numerical model is not limited by this fact, although the results show systematic upside deviations, compared with the experiments.

Probably the Joule heating has a less dominant effect than it was expected, because the heat loss to the filler material becomes more important in this range.

Therefore a more dimensional model with implicit numerical procedures is under development.

Another improvement of the model is planned by increasing the number of elements, as the convergence limit is not yet been reached in the case of the high current densities.

Conclusions.

The one dimensional numerical model describes the dynamical burnback processes within a wide range of current densities.

It indicates that the heat loss by conduction in the silver has a delaying influence on the burnback velocity, during a fraction of a ms at 1 kA/mm or during several ms at 0.1 kA/mm .

As a consequence, the mean burnback velocity which is determined experimentally after a relatively long arcing time, often will not correspond to the instantaneous velocity obtained after short arcing times.

For current densities above 3 kA/mm the present model predicts an exponential increase of the burnback velocity, although experiments show that this effect is less dramatic.

Acknowledgement.

The authors want to express their gratitude to Drs. A.J. Geurts of the Department of Mathematics of the Eindhoven University of Technology for his *stimulating remarks*.

References.

- [1] : Kroemer, H.: Der Lichtbogen an Schmelzleitern in Sand.
Arch.Elektrotechn. 36 (1942) 455-470.
- [2] : Daalder, J.E. and Schreurs, E.F.: Arcing Phenomena in High Voltage Fuses.
EUT Report 83-E-137. Eindhoven University of Technology (1983).

Session V

DEVELOPMENT AND DESIGN ASPECTS

Chairman: Prof. Dr. T. Lipski